Journal of Energy Storage 117 (2025) 116099

Contents lists available at ScienceDirect

Journal of Energy Storage

journal homepage: www.elsevier.com/locate/est

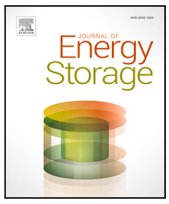

Research papers

Structural, electronic, and Li-ion adsorption properties of PolyPyGY explored by first-principles and machine learning simulations: A new multi-ringed 2D carbon allotrope

K.A.L. Lima [a,b], D.A. da Silva [c,d], G.D. Amvame Nze [c,d], F.L. Lopes de Mendonça [c,d], M.L. Pereira Jr [c], L.A. Ribeiro Jr [a,b,d,*]

[a] Institute of Physics, University of Brasília, 70910-900, Brasília, Brazil
[b] Computational Materials Laboratory, LCCMat, Institute of Physics, University of Brasília, 70910-900, Brasília, Brazil
[c] University of Brasília, College of Technology, Department of Electrical Engineering, University of Brasília, 70919-970, Brasília, DF, Brazil
[d] Professional Postgraduate Program in Electrical Engineering (PPEE), Department of Electrical Engineering, College of Technology, University of Brasília, Brasília, Federal District, Brazil

ARTICLE INFO

Keywords:
Polymerized Pyracyclene Graphyne (PolyPyGY)
2D carbon allotropes
Energy storage efficiency
Lithium-ion storage capacity
Optoelectronic properties

ABSTRACT

Two-dimensional (2D) carbon materials have been intensively investigated because of their distinctive structural framework and electronic behaviors as alternatives in energy conversion and storage applications. This study proposes a novel 2D carbon allotrope, Polymerized Pyracyclene Graphyne (PolyPyGY), characterized by a multi-ringed structure with 4-, 5-, 6-, 8-, and 16-membered rings comprising a porous structure. Using first-principles calculations and machine-learning techniques, we explore its structural, electronic, mechanical, optical, and lithium-ion storing properties. The vibrational properties assessed through the density functional perturbation theory framework confirm its structural stability. Moreover, ab initio molecular dynamics simulations at 1000 K demonstrate its thermal resilience, with no bond breaking or reconfiguration observed. The electronic band structure reveals a metallic nature, and the material exhibits anisotropic elastic properties, with Young's modulus varying between 421 and 664 GPa, suggesting good mechanical stability. Furthermore, lithium diffusion studies indicate low energy barriers (0.05-0.9 eV), max lithium-ion storage capacity of 2231.41 mAh/g, and a high diffusion coefficient ($> 6 \times 10^{-6}$ cm^2/s), along with a stable open circuit voltage of 2.5 V. These results highlight PolyPyGY's potential as a highly effective and durable anode material for lithium-ion batteries, featuring rapid Li-ion diffusion, stable intercalation, and consistent performance during charge and discharge cycles.

1. Introduction

Two-dimensional (2D) carbon-based materials have been extensively studied attributed to their exceptional structural and optoelectronic characteristics [1–4], including high surface area [5], excellent electrical [6] and thermal conductivity [7,8], and good mechanical resilience [9]. These properties make them promising candidates for various advanced technological applications [10]. Among these applications, using such materials as active layers in lithium-ion batteries (LIBs) stands out [11–14], where lithium storage capacity and ion diffusion speed are crucial factors for optimizing battery efficiency and durability.

The porous structure of 2D carbon materials, composed of varying-sized rings, enables a higher lithium adsorption capacity while facilitating Li diffusion across the material's surface [15]. These porous materials include allotropes such as graphyne [16], graphdiyne [17], and graphenylene [18], which, by presenting various carbon ring configurations, provide a structural network capable of stabilizing lithium insertion without compromising the material's mechanical integrity [19]. This feature is relevant for enhancing the capacity of LIBs, which are essential components in several energy storage technologies [20–26].

Recent studies on new 2D carbon allotropes have emphasized the need for structures that combine high adsorption capacity with optimized lithium diffusion barriers [27–40]. Such characteristics can

* Correspondence to: Institute of Physics, University of Brasília, Brasília, 70910-900, DF, Brazil.
E-mail address: ribeirojr@unb.br (L.A. Ribeiro Jr).

https://doi.org/10.1016/j.est.2025.116099
Received 10 December 2024; Received in revised form 14 February 2025; Accepted 2 March 2025
Available online 15 March 2025
2352-152X/

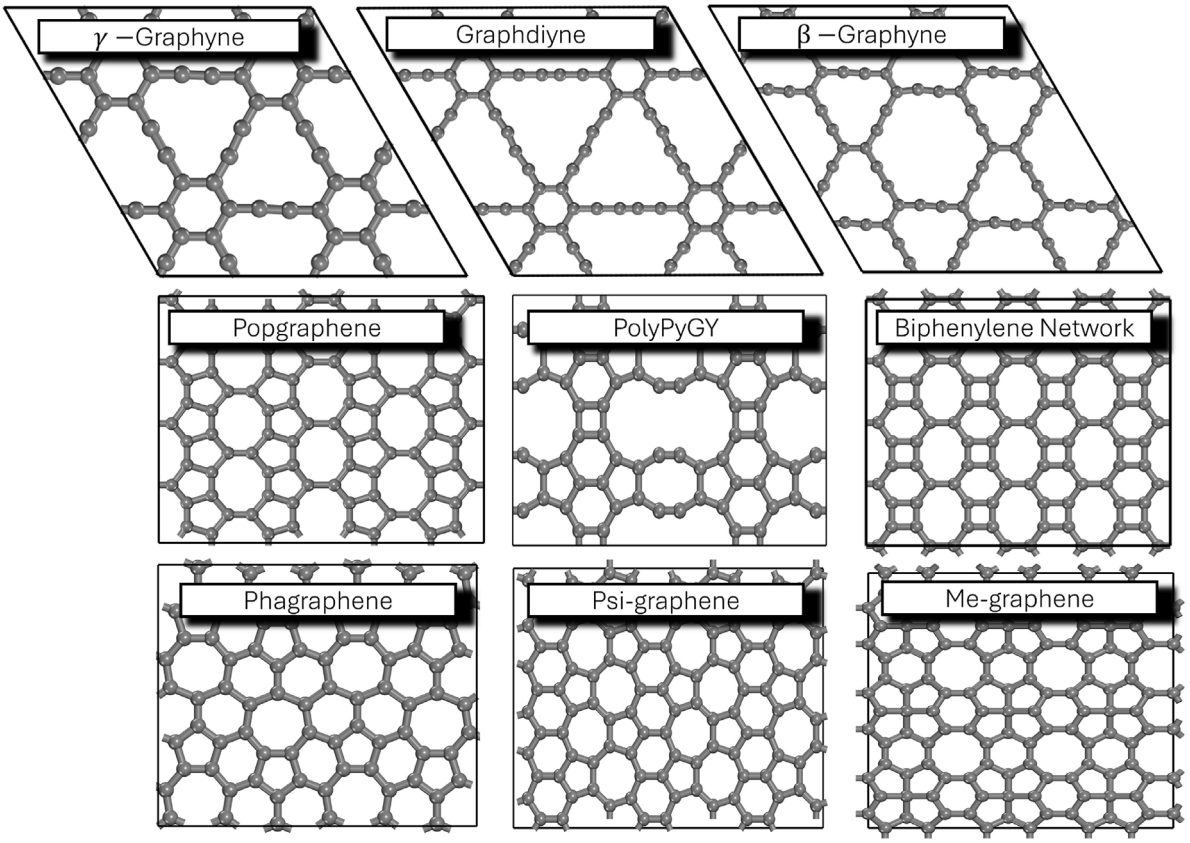

Fig. 1. Comparison of the atomic structures of PolyPyGY and other 2D carbon allotropes. The distinct ring arrangements and topologies highlight PolyPyGY's unique multi-ringed structure with 4-, 5-, 6-, 8-, and 16-membered rings, offering a balance of high porosity and structural stability advantageous for energy storage applications.

be achieved through structural configurations that maximize porosity, offering diverse adsorption sites and enabling efficient diffusion pathways. The nanomaterial proposed in this study, Polymerized Pyracyclene Graphyne (PolyPyGY), is a novel multi-ringed 2D all-carbon structure featuring 4, 5, 6, 8, and 16-membered rings, emerging as a promising response to these demands. Its porous structure with good thermal and mechanical stability has the potential to overcome limitations observed in conventional graphene-based allotropes when designing lithium-ion battery anodes [41].

Fig. 1 presents a comparative chart of PolyPyGY alongside a series of 2D carbon allotropes, including γ-graphyne [16], graphdiyne [17], β-graphyne [42], popgraphene [28], biphenylene network [43], phagraphene [44], psi-graphene [32], and Me-graphene [45]. These structures represent diverse topologies, ring arrangements, and bonding patterns, significantly influencing their mechanical, electronic, and adsorption properties. PolyPyGY distinguishes itself through its unique multi-ringed topology, characterized by a combination of 4-, 5-, 6-, 8-, and 16-membered rings. This structural arrangement provides high porosity while maintaining stability, which is advantageous for lithium-ion storage applications. In contrast, other allotropes such as graphdiyne and γ-graphyne feature uniformly distributed hexagonal and larger pores, which enhance their electronic conductivity but may limit their mechanical stability under extreme conditions [42].

Popgraphene and the biphenylene network exhibit smaller pore sizes and more uniform ring distributions, contributing to their exceptional mechanical properties but reducing their lithium-ion diffusion efficiency compared to PolyPyGY. Phagraphene and psi-graphene, with their mixed topologies, balanced porosity, and mechanical rigidity, lack the larger pores that facilitate enhanced ion mobility, as seen in PolyPyGY (discussed later). The β-graphyne and Me-graphene structures emphasize symmetry and uniformity, resulting in high thermal and mechanical stability. However, their limited porosity compared to PolyPyGY restricts their performance in energy storage applications, particularly for lithium-ion batteries, where higher adsorption capacity and ion diffusion are critical.

Herein, we investigate the structural, electronic, mechanical, optical, and lithium-ion adsorption properties of PolyPyGY using first-principles calculations and machine learning (ML) techniques. We examine its stability through phonon calculations and ab initio molecular dynamics (AIMD) simulations, characterize its electronic band structure, and assess its lithium diffusion barrier, adsorption capacity, and open-circuit voltage. This newly proposed 2D carbon allotrope originates from assembling dehydrogenated pyracyclene molecules [46, 47]. These molecules are interconnected by carbon atoms forming triple bonds in the x-direction, which create a highly stable and unique porous framework. This particular choice for including the triple bonds enables the formation of 16-membered rings with an adequate porous size for Li-ion storage. The design incorporates an innovative 8-membered ring conjunction that bridges neighboring pyracyclene-based motifs, resulting in a distinct topology. This assembly leads to a porous and robust architecture that balances mechanical stability with ample space for lithium adsorption. The combination of pyracyclene motifs and graphyne-like linkages enhances the material's electronic and adsorption properties, making PolyPyGY a promising high-performance anode material for LIBs, offering an ideal combination of fast Li-ion diffusion, stability, and storing capacity.

2. Methodology

To investigate the underlying physical, chemical, and lithium-ion adsorption properties of PolyPyGY, we employed first-principles calculations based on density functional theory (DFT) using the CASTEP code [48]. The initial atomic structure of PolyPyGY was optimized

using the Perdew–Burke–Ernzerhof (PBE) functional within the generalized gradient approximation (GGA) scheme for the exchange–correlation functional [49]. A plane-wave energy cutoff of 450 eV and a Monkhorst–Pack k-point mesh of 10 × 10 × 1 were applied for Brillouin zone sampling. Convergence criteria for energy and forces are 1.0×10^{-5} eV and 1.0×10^{-3} eV/Å, respectively. Structural relaxation employed periodic boundary conditions, ensuring minimal residual forces and pressure below 0.01 GPa. The vacuum space was set to 30 Å in the out-of-plane direction to avoid layer interaction. Phonon calculations were performed to confirm the structural stability of PolyPyGY, using density functional perturbation theory (DFPT), ensuring the absence of imaginary frequencies across the phonon dispersion spectrum. Importantly, van der Waals interaction corrections were considered within the Grimme D2 scheme [50].

Thermal stability was assessed via AIMD simulations at 1000 K, using a simulation time of 5 ps and a timestep of 1 fs. The AIMD simulations were conducted in the NVT ensemble with a Nosé–Hoover thermostat [51]. Throughout the simulation, we monitored the structural integrity to detect any bond breaking or atomic reconfiguration that could indicate thermal instability. The choice of the NVT ensemble was driven by the need to maintain a constant temperature during the simulations, which allows for accurate modeling of the system's thermal stability and ionic dynamics.

The electronic structure of PolyPyGY was analyzed by calculating the electronic band (using a k-point grid of 10 × 10 × 1) structure and density of states (DOS, using a k-point grid of 20 × 20 × 1). The partial density of states (PDOS) was also projected to identify contributions from specific atomic orbitals, providing insights into the material's conductive properties. Optical properties were explored under an external electric field using complex dielectric constant calculations [52].

Lithium adsorption studies were conducted by placing Li atoms at various adsorption sites on the PolyPyGY surface, followed by geometry optimization to identify energetically favorable configurations. The adsorption energy (E_{ads}) was calculated using the formula $E_{\text{ads}} = E_{\text{Li+PolyPyGY}} - \left(E_{\text{PolyPyGY}} + E_{\text{Li}}\right)$, where $E_{\text{Li+PolyPyGY}}$ is the total energy of PolyPyGY with adsorbed Li, E_{PolyPyGY} is the energy of pristine PolyPyGY, and E_{Li} is the energy of lithium atoms in the gaseous phase. We computed the diffusion barrier along possible migration paths using the nudged elastic band (NEB) method within CASTEP to investigate lithium diffusion [53–55]. The diffusion coefficient was estimated from these results, providing insights into lithium mobility on the PolyPyGY surface. The theoretical capacity of a material in LIBs refers to the maximum amount of electrical charge that can be stored per unit weight of the material during the complete lithiation process. It is a critical metric for assessing the energy storage potential of electrode materials. In this way, the theoretical capacity (C) was calculated using the equation: $C = N_{MAX}F/M$, where N_{MAX} is the maximum number of Li atoms adsorbed on PolyPyGY, F = 96485.332 sA/mol is the Faraday constant, and M is the molar mass of the PolyPyGY supercell.

The adsorption locator tool [56–58] within the Materials Studio suite was used to determine the most stable configuration at each lithium concentration on PolyPyGY. This tool enables the systematic exploration of potential adsorption sites. It evaluates their relative stability based on the calculated adsorption energies. Multiple configurations were generated and ranked for each concentration based on their total energies. The configuration with the lowest total energy was selected as the most stable. Possible adsorption configurations are identified by carrying out Monte Carlo searches of the configurational space of the substrate-adsorbate system as the temperature slowly decreases according to a simulated annealing schedule. This approach ensures we accurately identify the energetically favored lithium distribution in the PolyPyGY structure on each Li concentration. The supplementary material discusses the approach to determining the most stable configuration of the system at each Li concentration.

The mechanical behavior of PolyPyGY was investigated through classical reactive molecular dynamics simulations using the Large-scale Atomic/Molecular Massively Parallel Simulator (LAMMPS) software [59]. A reactive force field tailored specifically for PolyPyGY was derived from a moment tensor potential (MTP) [60], which was fitted to explore its mechanical properties with the assistance of the Moment Tensor Potential (MTP) model [61,62]. Our study evaluated the mechanical response of PolyPyGY using a Machine Learning Interatomic Potential (MLIP) based on MTP model. This model was generated by combining quantum-mechanical calculations with active learning, as implemented in the MLIP package [61,62].

Using an active learning protocol, the MTP model was designed and trained for the PolyPyGY structure, ensuring it accurately captured the material's potential energy surface (PES) under various conditions. The training dataset was generated through ab initio calculations performed with DFT within the GGA/PBE scheme. These calculations included configurations of strained supercells under uniaxial and biaxial deformations and at different temperatures, providing a diverse dataset representative of the material's mechanical behavior.

The training of the MTP model followed an active learning approach, which iteratively refined the model to improve its accuracy [60]. Initially, a small subset of DFT data was used for training. The model's uncertainty was then evaluated on unexplored configurations, identifying regions of high uncertainty in the PES. These high-uncertainty configurations were subsequently included in the training dataset through additional DFT calculations, enabling the model to generalize well across diverse strain and temperature conditions. This iterative process ensured a comprehensive and accurate representation of PolyPyGY's structural responses.

Importantly, the accuracy of the MTP model was validated against an independent DFT dataset. The validation metrics demonstrated that the model achieved a mean absolute error (MAE) of 2.0 meV/atom for energy and 0.05 eV/Å for forces, confirming its reliability [60]. Additionally, the training and validation loss curves as functions of iterations showed stable convergence, further supporting the robustness of the training process, as shown in the supplementary material.

The trained MTP model was subsequently employed in large-scale molecular dynamics simulations, as discussed below, to investigate PolyPyGY's stress–strain behavior. These simulations enabled the efficient calculation of mechanical properties, such as anisotropic Young's modulus, tensile strength, and failure strain, while maintaining quantum-mechanical accuracy. By bridging the gap between computational efficiency and quantum-level precision, the MTP model provided valuable insights into this novel material's mechanical response.

AIMD simulations were conducted following the same parameters used previously, employing the Vienna Ab initio Simulation Package (VASP) [63–65]. The training dataset for the MTP-based MLIP was constructed using stress-free and uniaxially strained supercells at various temperatures, an approach that has been successfully applied in recent studies to generate MLIPs for complex materials [66–74].

For the MTP, a cutoff distance of 3.5 Å was established, and training was performed using a two-step passive training approach, as described in recent literature [71]. Newton's equations of motion were integrated using the velocity Verlet algorithm with a timestep of 0.05 fs. Thermalization and stress relaxation were achieved through the thermostat and NPT ensemble simulations throughout 100 ps. We adopt the NPT ensemble to allow pressure equilibration and a more realistic treatment of lattice relaxation under uniaxial strain rate conditions. The elastic properties and fracture behavior of the PolyPyGY sheet were assessed at 300 K, where the material was subjected to uniaxial tension using a constant engineering tensile strain rate of 10^{-6} fs^{-1}.

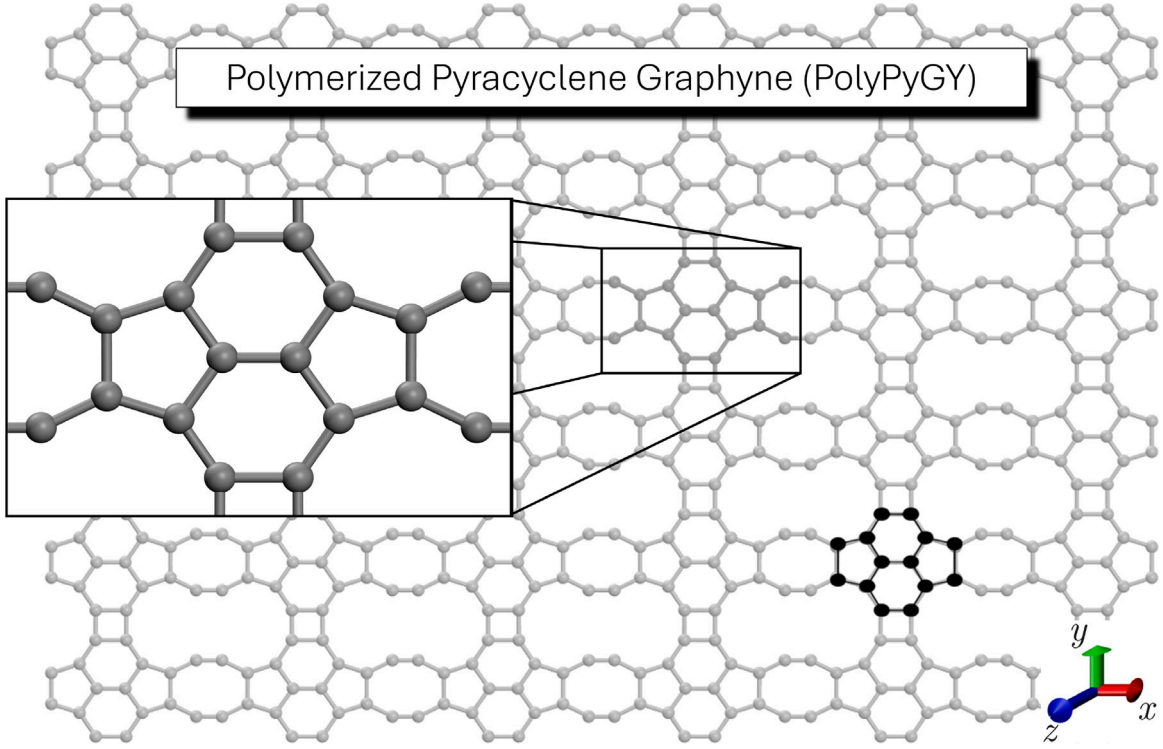

Fig. 2. Atomic structure of PolyPyGY. The unit cell, outlined in black, has dimensions of $a = 9.46$ Å (x-direction) e $b = 6.08$ Å (y-direction). The black spheres denote the structure of a dehydrogenated pyracyclene molecule. (For interpretation of the references to color in this figure legend, the reader is referred to the web version of this article.)

3. Results

The atomic structure of PolyPyGY is presented in Fig. 2. As depicted, the lattice is composed of 4-, 5-, 6-, 8-, and 16-membered rings of carbon atoms, forming a highly porous structure. The unit cell, highlighted in black, contains 18 atoms with dimensions $a = 9.46$ Å (x-direction) e $b = 6.08$ Å (y-direction). The C–C bond lengths vary slightly across the structure, with typical values ranging between 1.38 Å to 1.48 Å, corresponding to different bonding environments between carbon atoms in the various ring sizes. Crystallographically, PolyPyGY belongs to the PMMM space group and adopts a D2H-1 symmetry.

The calculated formation energy for PolyPyGY is −8.44 eV/atom, indicating good energetic stability. This value is comparable to other 2D carbon allotropes, such as biphenylene network (−7.42 eV/atom) [75], graphene (−8.83 eV/atom) [76], sun-graphyne (−8.57 eV/atom) [77], irida-graphene (−6.96 eV/atom) [78], and dodecanophene (−8.19 eV/atom) [79]. It is significantly more stable than other porous allotropes, like graphdiyne (−0.77 eV/atom) and γ-graphyne (−0.92 eV/atom) [80]. The lattice of PolyPyGY appears perfectly planar, with no observed buckling deformations. PolyPyGY's multi-ringed architecture, especially larger 16-membered rings, significantly contributes to its high porosity and large surface area, which are advantageous for lithium-ion storage and diffusion applications. This unique atomic arrangement also supports robust mechanical stress, as discussed later.

Fig. 3 presents the phonon dispersion results for PolyPyGY, showcasing its dynamic stability. The dark and light blue lines show the phonon calculations performed using DFPT and the MTP methods [81]. In both results, the absence of imaginary frequencies across the phonon spectrum suggests the dynamic stability of PolyPyGY. The MTP-based phonon calculations (light blue) strongly agree with the DFPT (dark blue) results, validating the accuracy of the MTP-based generated MLIP for PolyPyGY. The alignment of results from DFPT and MTP further supports the use of ML-based potentials here and in future studies focused on the mechanical and thermal behavior of PolyPyGY using classical reactive MD simulations. Also, the consistency between these two methods can enable efficient simulations of larger systems and longer timescales without sacrificing accuracy.

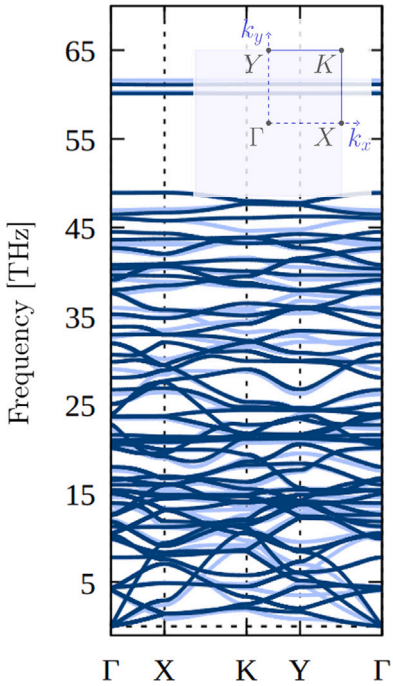

Fig. 3. Phonon dispersion analysis of PolyPyGY calculated using DFPT (dark blue) and MTP (light blue) methods. The inset highlights the first Brillouin zone. (For interpretation of the references to color in this figure legend, the reader is referred to the web version of this article.)

In Fig. 4, the thermal stability of PolyPyGY is assessed through AIMD simulations at 1000 K. Insets show top and side views of the

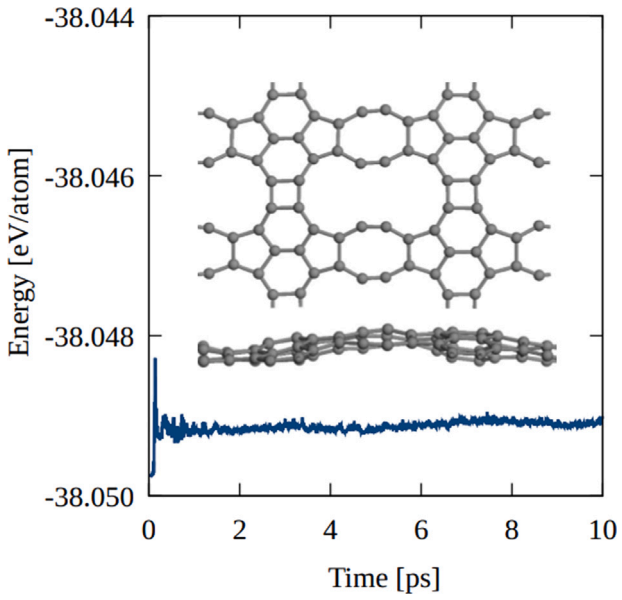

Fig. 4. The AIMD simulation results at 1000 K, depicting the lattice total energy as a function of time. Insets show top and side views of the structure for the final AIMD snapshot at 5 ps.

structure for the final AIMD snapshot at 10 ps. This thermal regime is commonly used to assess the intrinsic thermal stability of novel materials, providing insights into their resilience under extreme conditions. Demonstrating good thermal stability at 1000 K opens avenues for exploring PolyPyGY potential in applications beyond LIBs. The absence of bond breaking or structural reconfiguration in the insets indicates that PolyPyGY remains thermally stable under high-temperature conditions. This stability is critical for practical applications, especially in environments where materials are subjected to significant thermal stress, such as LIB anodes. The insets also show that the lattice maintains its integrity without any observable in-plane and drastic out-of-plane deformation.

Now, we turn to the electronic properties of the proposed nanomaterial. Fig. 5 shows these properties for pure PolyPyGY (dark blue) and the lattice containing one adsorbed Li atom (PolyPyGY@Li, light blue). In Fig. 5(a), the electronic band structure is shown along high-symmetry k-paths, revealing that PolyPyGY exhibits a metallic nature. PolyPyGY can conduct electrons efficiently, making it suitable for applications requiring controlled electronic transport. Fig. 5(b) presents the PDOS, where only contributions from p atomic orbitals are visible for the depicted range of energies. The PDOS confirms the dominant orbital contributions, such as carbon p-orbitals near the Fermi level, consistent with the PolyPyGY's metallic character.

The band structure of PolyPyGY exhibits a downward shift in energy levels upon lithium adsorption. This shift arises from the charge transfer process, where lithium donates electrons to the PolyPyGY lattice. As a result, the Fermi level value increases, stabilizing the electronic structure by redistributing charge within the conduction band. This behavior confirms the material's ability to accommodate lithium ions and underscores its suitability as a potential anode material for lithium-ion batteries.

Figs. 5(c,d) show the highest occupied crystalline orbital (HOCO, red) and the lowest unoccupied crystalline orbital (LUCO, green). The spatial distribution of these orbitals indicates that HOCO delocalizes on the 5- and 8-membered rings while LUCO concentrates in 4- and 6-membered rings, revealing distinct electron and hole transport channels across the material. The HOCO and LUCO distributions suggest that PolyPyGY could support efficient and controllable charge transport, further supporting its potential use in conductive layers for energy storage devices. The orbital distribution in pristine PolyPyGY (Fig. 5(a)) undergoes significant changes upon lithium adsorption, as shown in Fig. 5(d). the polarization effects induced by the lithium atom and minor structural distortions in the material further enhance the confinement of electronic states in its vicinity. Consequently, the adsorption process increases the localization of the LUCO around the lithium atom.

PolyPyGY exhibits interesting optical characteristics, with polar ization-dependent profiles along the x-direction (dark blue) and y-direction (light blue), as illustrated in Fig. 6. In Fig. 6(a), the absorption coefficient (α) is plotted against photon energy, revealing broad optical responses with peaks in the visible to ultraviolet (UV) range. The absorption coefficient reaches values exceeding 10^4 cm^{-1}, indicating the material's high absorption efficiency at these wavelengths. These intense and broad absorption trends suggest that PolyPyGY could be advantageous in optoelectronic applications, where effective light capture in a wide spectrum range is desirable.

Fig. 6(b) shows reflectivity (R) results. The material exhibits low reflectivity across the studied energy range, remaining below 0.9, which implies that a significant amount of incident light is transmitted rather than reflected. The clear anisotropic nature of R hints at potential uses in applications that benefit from directional light transmission, making PolyPyGY a candidate for selective optical coatings or filters. The refractive index (η) in Fig. 6(c) also displays polarization-dependent behavior, gradually decreasing with photon energy and converging near 1.0 at higher energies (around 10 eV). This trend indicates birefringent properties in PolyPyGY, once η varies with light polarization. This anisotropic trend enhances the PolyPyGY's versatility for applications rely on controlled light propagation.

PolyPyGY has not yet been synthesized or studied experimentally. These electronic and optical results provide a theoretical foundation for understanding PolyPyGY's properties, guiding future experimental investigations. For instance, experimental synthesis could be pursued using bottom-up techniques such as dehydrogenating pyracyclene molecules, as outlined in the "Introduction" section. This approach could provide samples for further characterization. Techniques such as UV–Vis spectroscopy and photoluminescence measurements could validate the computed optical absorption spectra, particularly in the visible and ultraviolet regions. Angle-resolved photoemission spectroscopy (ARPES) could be used to measure the electronic band structure, providing direct experimental insights into the material's metallic nature and density of states.

The mechanical response of PolyPyGY under uniaxial stress evaluated using the MLIP method is illustrated in Fig. 7. The stress–strain curve, plotted for the x-direction (dark blue) and y-direction (light blue), reveals the material's anisotropic mechanical responses under uniaxial tensile loading, as evidenced by the distinct responses along these two orientations. The stress increases linearly with strain initially, indicating elastic behavior. At higher strain values, a peak is observed, representing the maximum stress (ultimate strength) that PolyPyGY can withstand before undergoing fracture.

In the x-direction, PolyPyGY reaches maximum (ultimate) stress at approximately 80 GPa for 14.3% of strain (fracture strain, dashed dark blue line). In contrast, the ultimate stress is substantially different in the y-direction, reaching approximately 40 GPa at 11.3% of strain (fracture strain, dashed light blue line). This anisotropy in the mechanical response is likely due to the structural orientation of PolyPyGY's ring configuration, which affects bond stretching and deformation under applied stress.

From the stress–strain curves shown in Fig. 7, Young's modulus of PolyPyGY is determined to be 421.90 GPa in the y-direction and 663.48 GPa in the x-direction, also indicating anisotropic mechanical behavior. These values suggest that PolyPyGY is a relatively stiff material. However, Young's modulus is lower than that of graphene, which has a modulus close to 1 TPa in both directions [82,83]. This difference can be attributed to PolyPyGY's porous, multi-ring structure, which, while providing rigidity, introduces greater flexibility compared to graphene's

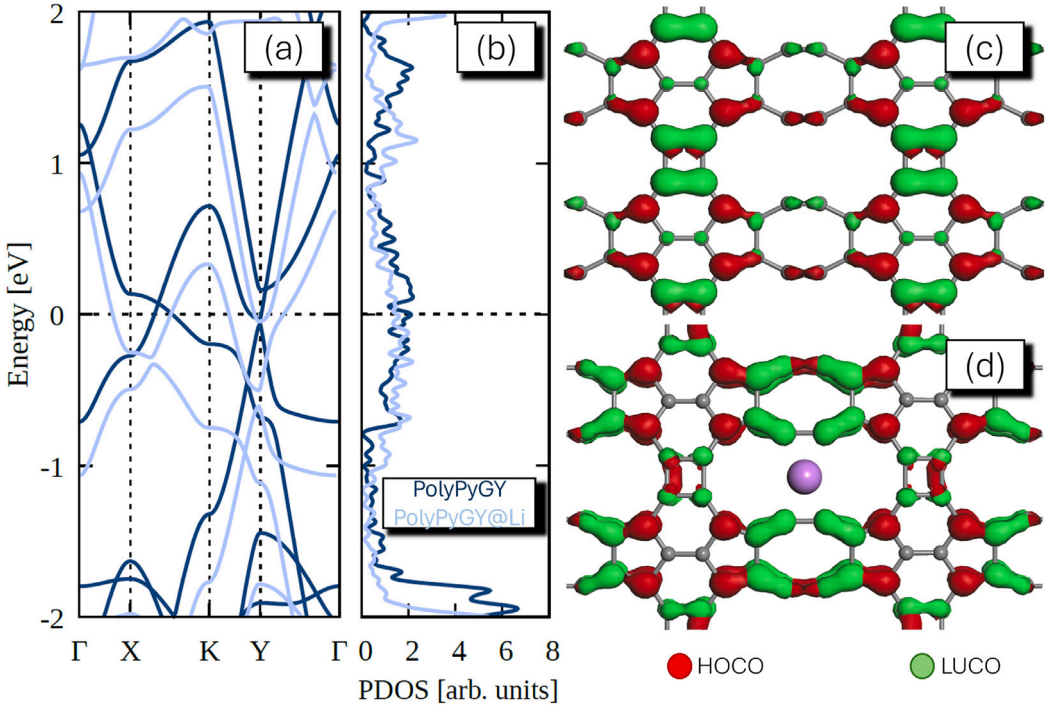

Fig. 5. Electronic structure of PolyPyGY. (a) Band structure along high-symmetry k-paths and (b) PDOS. Panels (c) and (d) depict the Highest Occupied Crystalline Orbital (HOCO, red) and Lowest Unoccupied Crystalline Orbital (LUCO, green) distributions for PolyPyGY and PolyPyGY@Li, respectively. (For interpretation of the references to color in this figure legend, the reader is referred to the web version of this article.)

continuous, denser hexagonal network. The anisotropy in PolyPyGY, with higher stiffness along the x-direction, reflects the alignment of its ring structures, influencing its ability to accommodate deformation.

Fig. 8 illustrates the fracture patterns and stress distribution in PolyPyGY under uniaxial strain applied in the x and y directions. The von Mises stress (σ^{VM}) distribution [84], shown with a color gradient from blue (low stress) to red (high stress), reveals how strain impacts different regions of the lattice at various deformation stages, highlighting the material's fracture behavior.

The initially unstressed PolyPyGY lattice is shown in Fig. 8(a). In Fig. 8(b), where the structure is stretched along the x-direction, stress concentrations initially form around the larger rings and multi-ring junctions, and the first bonds break for a fracture of strain of 14.3%. By 14.4% strain (Fig. 8(c)), these stress concentrations initiate micro-cracks in a parallel direction (y-direction) regarding the tensile loading direction. These micro-cracks propagate for higher strain (ϵ) values, coalescing into more extensive fractures and eventually causing significant rupture across the lattice. This behavior indicates that the structural features aligned along the x-direction, such as the larger rings, act as weak points under tensile stress, guiding the fracture pathways along these regions.

With strain applied along the y-direction, a similar pattern emerges but with different fracture dynamics due to the orientation of the rings relative to the applied stress. At 11.3% strain (see Fig. 8(d)), stress accumulates more uniformly, but by 11.4% strain, localized stress concentrations lead to fast crack propagation perpendicularly to the strain. These areas experience significant bond rupture, leading to an extended network of fractures. The directional dependence observed in the fracture patterns highlights the anisotropic nature of PolyPyGY, as the structure's response to stress varies markedly between the x and y directions.

Finally, we discuss the Li-ion adsorption properties of PolyPyGY. Fig. 9 comprehensively analyzes the lithium adsorption and diffusion behavior on the PolyPyGY surface. Fig. 9(a) shows the adsorption energy landscapes with pathways for a single Li atom diffusion on the PolyPyGY surface, revealing preferential adsorption sites with negative adsorption energies. The calculated adsorption energies range between −2.3 to −0.93 eV, indicating strong binding of Li to specific lattice regions. These values are comparable to [85–88] or better [29,30,40, 89–91] than other 2D carbon allotropes (including graphene, about −1.57 eV [92]), demonstrating PolyPyGY's ability to stably adsorb Li ions without compromising structural integrity.

As shown in Fig. 9(b), energy profiles for lithium diffusion highlight the low barriers facilitating efficient ion mobility on the surface [93]. Importantly, each pathway's minimum energy path profile was fitted using a second-order polynomial equation containing five points, two on the left and two on the right of the maximum value. The colored lines refer to the colored arrows in Fig. 9(a). Varying between 0.10 and 0.92 eV, these diffusion barriers are among the lowest observed for other 2D carbon allotropes [29,30,40,85–91], reflecting the synergy between PolyPyGY's porous network and its electronic structure. The barriers' directional dependence emphasizes the material's anisotropic nature, which could be leveraged to optimize ion transport along specific pathways. The relative energy for each diffusion path is calculated based on the energy of the most stable adsorption site along that path. Additionally, to ensure all energy values are positive and visually consistent, we added the absolute value of this adsorption energy to all other values.

Figs. 9(c,d) provide further insights into lithium migration in Poly PyGY, explicitly focusing on possible transitions between the 16-mem bered rings. These new panels complement the previously discussed pathways by analyzing the energy barriers associated with lithium-ion movement through different structural configurations. In Fig. 9(c), the diffusion pathways are represented by various dotted arrows, each corresponding to a distinct lithium migration route. The green and red pathways exhibit the highest energy barriers, reaching 1.38 eV and 2.0 eV, respectively (see Fig. 9(d)). These elevated energy barriers suggest that structural constraints within the lattice hinder lithium migration along these paths. The red pathway, in particular, likely encounters a bottleneck effect due to the limited spatial freedom available for the lithium-ion as it moves between adjacent 16-membered rings. Similarly, the green pathway may be restricted by steric hindrance or local charge redistribution effects that increase the energy cost of migration.

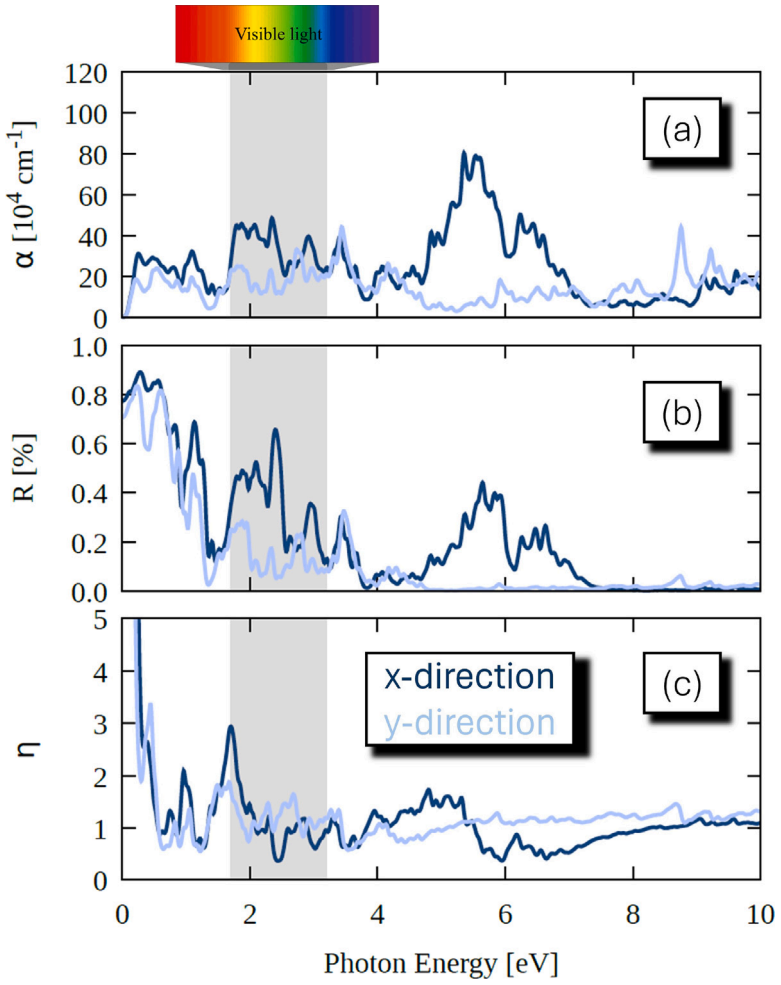

Fig. 6. Optical properties of PolyPyGY. (a) Absorption coefficient (α), (b) reflectivity (R), and (c) refractive index (η) as a function of photon energy and for light polarized along the x-direction (dark blue) and y-direction (light blue). (For interpretation of the references to color in this figure legend, the reader is referred to the web version of this article.)

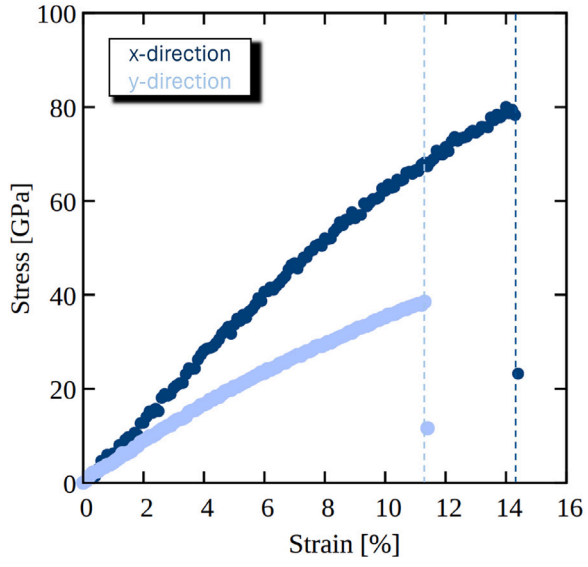

Fig. 7. Stress–strain curve of PolyPyGY under uniaxial stress in the x-direction (dark blue) and y-direction (light blue), calculated using the MLIP method. (For interpretation of the references to color in this figure legend, the reader is referred to the web version of this article.)

The corresponding energy profiles for lithium diffusion along these pathways are shown in Fig. 9(d). The highest energy barriers (red and green) indicate that Li migration across these paths is less favorable, requiring considerable activation energy for the ion to transition between adjacent sites. In contrast, the black and blue diffusion pathways display energy barriers comparable to some of those observed in Fig. 9(b) for alternative transitions. This observation implies that lithium migration within PolyPyGY primarily follows lower-energy routes, favoring in-plane diffusion over direct transitions between 16-membered rings. The existence of relatively low-barrier pathways (black and blue) further supports the idea that lithium mobility in PolyPyGY is not strictly confined but instead follows an interconnected network of energetically accessible migration channels.

Fig. 10 depicts the energy profile and barrier for lithium diffusion across the PolyPyGY surface and the temperature-dependent diffusion coefficients [27] for all the pathways studied here, which underscore PolyPyGY's performance under various operating conditions. Fig. 10(a) provides a 3D structural representation of the diffusion pathway (indicated by the purple arrow), showing a lithium atom traversing along the material's surface. Fig. 10(b) shows the corresponding energy profile for lithium-ion diffusion along this pathway, plotted as a function of the diffusion coordinate.

The energy profile reveals a peak energy barrier of 0.86 eV, indicating the energy required for the lithium atom to transition between adjacent stable adsorption sites. This energy barrier is slightly lower than the barrier observed for diffusion through the 16-membered ring,

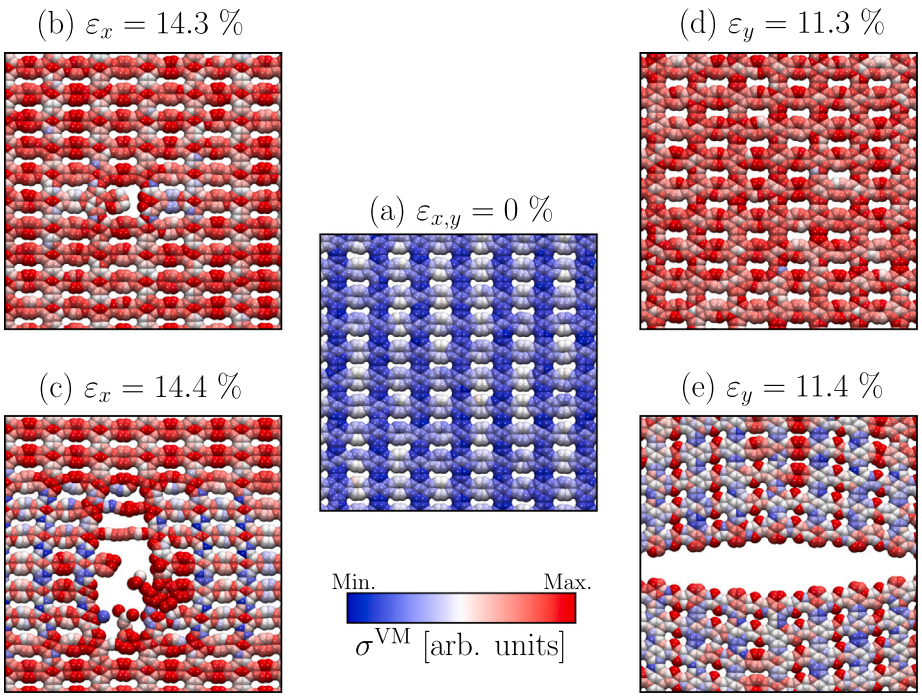

Fig. 8. Fracture patterns and stress distribution in PolyPyGY, initially unstressed in panel (a), under uniaxial strain in the *x*-direction (panels b and c) and *y*-direction (panels d and e). The von Mises stress distribution is illustrated with a color gradient, where blue represents low stress and red indicates high stress. (For interpretation of the references to color in this figure legend, the reader is referred to the web version of this article.)

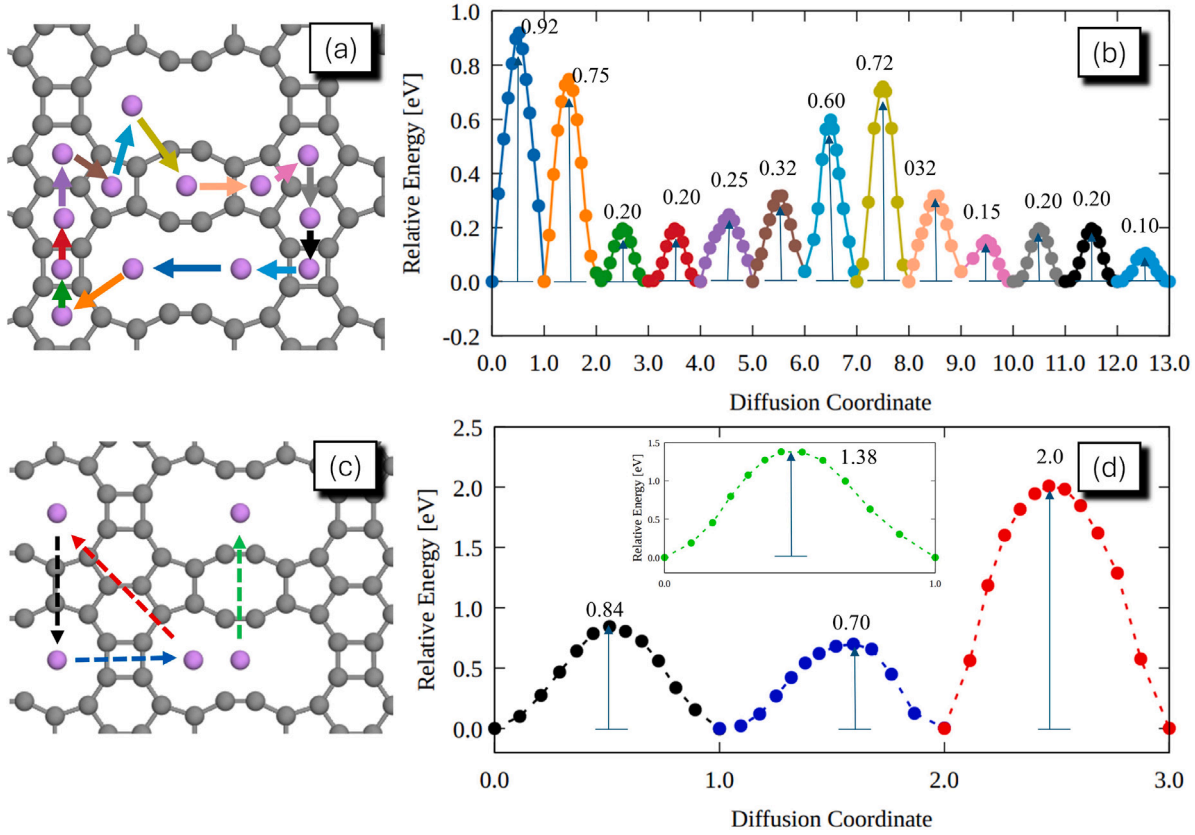

Fig. 9. Lithium adsorption properties of PolyPyGY. (a,c) Adsorption energy landscape and pathways for a single Li atom on the PolyPyGY surface and (b,d) energy profile for Li diffusion along a selected pathway. The colored lines in panels (b,d) refer to the colored arrows in panels (a,c). (For interpretation of the references to color in this figure legend, the reader is referred to the web version of this article.)

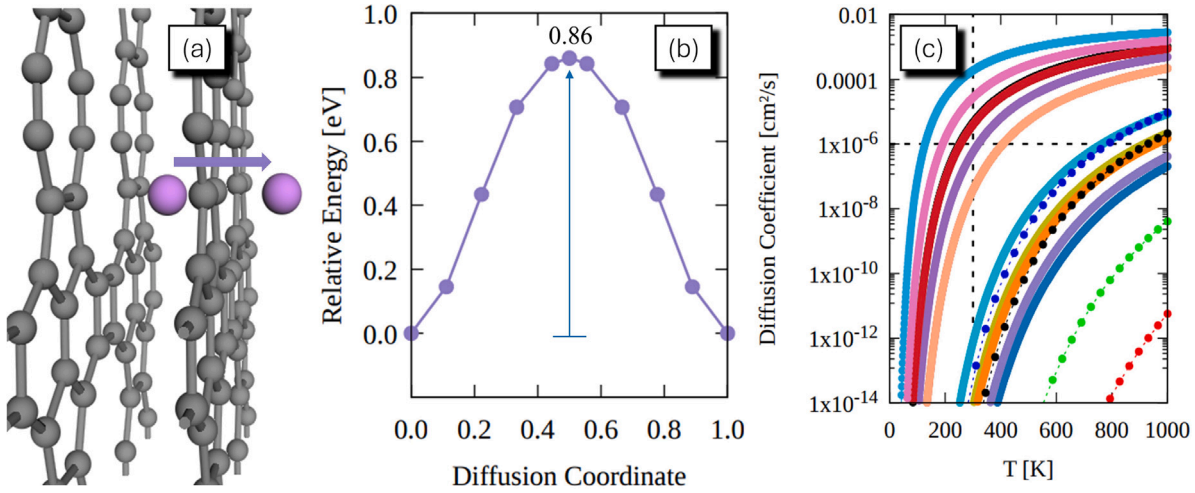

Fig. 10. Lithium adsorption and diffusion properties of PolyPyGY. (a) Adsorption energy pathway for a single Li atom across the PolyPyGY surface, (b) energy profile for Li diffusion along the selected pathway, and (c) temperature-dependent diffusion coefficients. The dashed lines in panel (c) represent the graphene diffusion coefficient at room temperature. The colored lines in panels (c) refer to the colored arrows in panels (a,c) of Fig. 9 and (b) of this figure. (For interpretation of the references to color in this figure legend, the reader is referred to the web version of this article.)

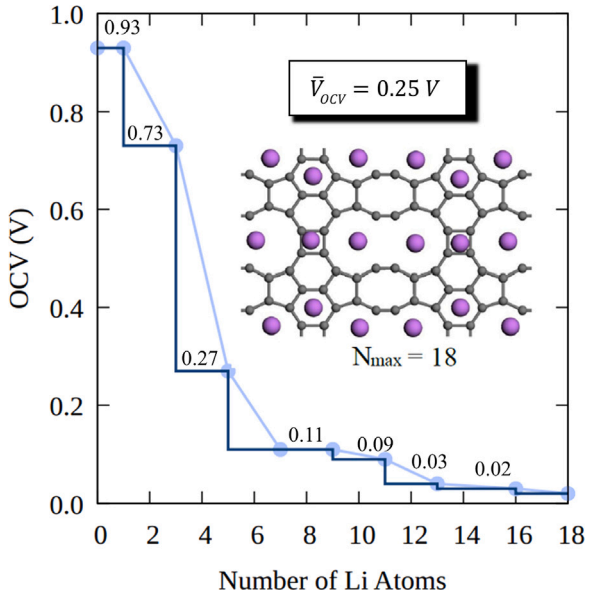

Fig. 11. OCV as functions of the number of adsorbed in PolyPyGY. The average OCV is 0.25 eV.

demonstrating that the surface of PolyPyGY provides a more energetically favorable environment for lithium migration than the interior pore pathways. The dashed lines in Fig. 10(c) represent the graphene diffusion coefficient at room temperature for comparison. The colored lines refer to the colored arrows in Figs. 9(a,c) and 10(a). At room temperature, the diffusion coefficient surpasses 6×10^{-6} cm^2/s, indicative of excellent Li-ion mobility [94,95]. As temperature increases, the exponential growth in diffusion coefficients confirms the thermal activation of Li-ion dynamics, further validating PolyPyGY's suitability for high-efficiency LIBs.

One can also note that the diffusion coefficient results in Fig. 10(c) for the Li migration between adjacent 16-membered rings align with the observed energy barriers in Fig. 9(d). As expected, the diffusion coefficients corresponding to the highest energy barriers (1.38 eV and 2.0 eV, represented by the dotted green and red lines) exhibit the lowest values across the temperature range. This behavior reinforces the notion that lithium migration through these pathways is highly hindered, likely due to steric effects and the structural constraints imposed by the surrounding carbon framework. In contrast, the diffusion coefficients associated with the lower energy barriers, such as those following the dotted black and blue migration paths, are significantly higher, suggesting that lithium prefers these lower-energy pathways for migration, with preferred migration channels between neighboring adsorption sites.

The interplay between open circuit voltage (OCV) and the number of lithium atoms is presented in Fig. 11. The OCV values were calculated using the method described in Ref. [27]. One can note a clear trend as adsorbed lithium atoms increase. The initial adsorption energy is highly negative, indicating strong binding at low Li coverage. As the lithium coverage increases, the adsorption energy gradually increases, stabilizing near −2.3 eV at 18 Li atoms, as mentioned above. This behavior reflects the increasing electrostatic repulsion and site competition among Li atoms as more are adsorbed. Despite this, PolyPyGY maintains strong adsorption even at high lithium concentrations, suggesting that its porous and multi-ringed structure effectively accommodates Li ions without compromising binding stability.

PolyPyGY's average OCV is approximately 0.25 eV, positioning it among materials with relatively low OCV values compared to other 2D carbon-based allotropes. This trend makes it attractive for acting as an anode in Li-ion battery applications. Low OCVs are generally better for anodes since they minimize the voltage difference between the anode and the Li-ion agglomerate, improving efficiency. A low OCV also reduces the risk of lithium plating during charging and ensures the battery can store more energy effectively.

Graphene, for instance, exhibits an OCV of 0.11 eV [96], while graphite has an OCV ranging from 0.22 to 0.40 eV [97]. These values suggest that PolyPyGY demonstrates comparable electrochemical stability and is suitable for Li-ion battery applications. However, compared to TPDH-graphene and twin-graphene, which exhibit OCVs as low as 0.29 eV [27] and 0.32 eV [98], respectively, PolyPyGY offers a competitive balance between stability and energy density. Materials with higher OCV values, such as QPHT-graphene (0.66 eV) [99] and popgraphene (0.45 eV) [28], are more suitable for cathode applications but may present challenges for anode usage due to their higher initial voltage requirements. The low average OCV of PolyPyGY reflects its potential as an anode material, ensuring a stable intercalation voltage that is less likely to lead to lithium plating during charge cycles. This property, combined with its metallic nature and favorable diffusion barriers, underscores PolyPyGY's versatility and efficacy in advanced energy storage systems.

The theoretical capacity of PolyPyGY in storing lithium ions, calculated to be 2231.41 mAh/g, far surpasses some of the 2D carbon-based allotropes referenced here. For example, graphene exhibits a much lower capacity of 568 mAh/g [96], and graphite, commonly used in commercial lithium-ion batteries, only has 372 mAh/g capacity [97]. Among the moderate-capacity materials, graphenylene and popgraphene offer capacities of 1116 mAh/g [19] and 1487 mAh/g [28], respectively. However, these values still fall significantly short of PolyPyGY's capacity. Twin-graphene, for instance, exhibits a remarkable capacity of 3916 mAh/g [98], much higher than PolyPyGY.

PolyPyGY's good capacity can be attributed to its unique multi-ringed porous structure, which provides abundant adsorption sites for lithium ions. This structural advantage makes PolyPyGY a competitive candidate for next-generation lithium-ion battery anodes, combining high theoretical capacity with its moderate OCV (0.25 eV). Such a balance between capacity and electrochemical stability is crucial for ensuring high energy density and long-term cycling performance in practical applications.

Wettability plays a critical role in determining the performance of LIBs. PolyPyGY is a graphyne-based structure, and previous studies have demonstrated that graphyne exhibits favorable properties for electrolyte compatibility and wettability. A study by Bagheri et al. [100] showed that graphyne is more hydrophobic than graphene but still facilitates the formation of a water sublayer, enhancing interaction with liquid electrolytes. Using molecular dynamics, Chagas et al. [101] highlighted the compatibility of graphyne with biocompatible ionic liquids, showing higher capacitance and stable electrolyte-electrode interactions compared to graphene. Fluorine-doped graphyne has been reported by Lee et al. [102] to enhance ionic and electrical conductivity, further improving electrolyte compatibility and electrochemical performance. These studies collectively suggest that PolyPyGY, as a graphyne-like structure, is likely to exhibit good compatibility with common electrolytes, benefiting from its porosity, surface structure, and interaction capabilities.

Importantly, we have assessed the thermal stability of the PolyPyGY when fully loaded with lithium atoms at its maximum adsorption capacity (18 atoms) as determined by AIMD simulations conducted at 300 K for a total duration of 10 ps (see supplementary material). Overall, PolyPyGY remains stable throughout the simulation, with minimal fluctuations in the total energy profile. No significant clustering or detachment of lithium atoms was observed (see video01.mp4 and video02.mp4 in the supplementary material). The lithium atoms remain well-bound to the material without inducing any substantial deformation or disruption to the planar structure of PolyPyGY.

4. Conclusion

This study presented Polymerized Pyracyclene Graphyne, a novel 2D carbon allotrope, as a promising candidate for LIB anodes due to its unique structural, electronic, mechanical, and electrochemical properties. PolyPyGY's multi-ringed architecture, composed of 4-, 5-, 6-, 8-, and 16-membered carbon rings, ensures structural stability and provides high porosity and diverse adsorption sites, critical for efficient lithium storage and transport. We demonstrated PolyPyGY's excellent structural stability through DFT and machine learning approaches. The material exhibits anisotropic mechanical properties. Young's modulus values of 421 GPa in the y-direction and 664 GPa in the x-direction offer both rigidity and flexibility suitable for diverse applications.

PolyPyGY's electronic structure, characterized by metallic behavior, ensures efficient charge transport, while the strong adsorption energies (−2.3 to −0.93 eV) and low diffusion barriers (0.05 to 0.9 eV) facilitate rapid Li-ion mobility. The material's high diffusion coefficient, exceeding 6×10^{-6} cm^2/s at 300 K, underscores its ability to support fast charge and discharge cycles. Furthermore, its average open circuit voltage (0.25 eV), stabilizing around 0.02 eV at higher lithium coverage, and its theoretical capacity for Li-ion storing (about 2231.41 mAh/g) confirm its suitability for high-capacity energy storage applications.

The inclusion of rings with 4, 5, 6, 8, and 16 members to compose PolyPyGY was guided by the following considerations:

- **Structural Stability:** Pyracyclene motifs interconnected by graphyne-like triple bonds minimize strain and maximize π-electron delocalization. Phonon dispersion and ab initio molecular dynamics (AIMD) simulations confirm this structure's thermodynamic and dynamic stability;
- **Electronic Properties:** As confirmed by our band structure calculations, the integration of pyracyclene motifs and graphyne-like linkages disrupts periodicity, enhancing electronic conductivity and providing a tunable density of states;
- **Mechanical Properties:** The diverse ring topology imparts anisotropic elastic properties, offering mechanical versatility;
- **Porosity:** The 16-membered rings, supported by the pyracyclene-based motifs, enhance porosity, facilitating lithium-ion diffusion and adsorption.
- **Design Motivation:** This combination of structural features was purposefully chosen to optimize lithium-ion storage properties. The porous framework and electronic conductivity allow for efficient lithium-ion diffusion, while the mechanical robustness ensures stability under lithiation.

These unique attributes, derived from the structural synergy of pyracyclene motifs and graphyne-like linkages, make PolyPyGY a promising high-performance anode material for LIBs. The material offers an ideal combination of fast Li-ion diffusion, structural stability, and high storage capacity.

CRediT authorship contribution statement

K.A.L. Lima: Writing – original draft, Visualization, Software, Methodology, Funding acquisition, Formal analysis, Data curation. **D.A. da Silva:** Writing – original draft, Visualization, Software, Methodology, Funding acquisition, Formal analysis, Data curation. **G.D. Amvame Nze:** Writing – original draft, Visualization, Software, Methodology, Funding acquisition, Formal analysis, Data curation. **F.L. Lopes de Mendonça:** Writing – review & editing, Funding acquisition, Conceptualization. **M.L. Pereira:** Writing – original draft, Visualization, Software, Methodology, Funding acquisition, Formal analysis, Data curation. **L.A. Ribeiro:** Writing – review & editing, Funding acquisition, Conceptualization.

Declaration of competing interest

The authors declare the following financial interests/personal relationships which may be considered as potential competing interests: Luiz A. Ribeiro Junior reports financial support was provided by Foundation for Research Support of the Federal District. Luiz A. Ribeiro Junior reports financial support was provided by National Council for Scientific and Technological Development.

Acknowledgments

This work received partial support from Brazilian agencies CAPES, CNPq, and FAPDF. L.A.R.J. acknowledges the financial support from FAP-DF grants 00193.00001808/2022-71 and 00193-00001857/2023-95, FAPDF-PRONEM grant 00193.00001247/2021-20, PDPG-FAPDF-CAPES Centro-Oeste 00193-00000867/2024-94, and CNPq grants 350176/2022-1 and 167745/2023-9. M.L.P.J. acknowledges the financial support of the FAP-DF grant 00193-00001807/2023-16. M.L.P.J. and L.A.R.J. thanks also to CENAPAD-SP (National High-Performance Center in São Paulo, State University of Campinas – UNICAMP, projects: proj960 and proj634, respectively) and NACAD (High-Performance

Computing Center, Lobo Carneiro Supercomputer, Federal University of Rio de Janeiro – UFRJ, projects: a22002 and a22003, respectively) for the computational support provided. The authors acknowledge the National Laboratory for Scientific Computing (LNCC/MCTI, Brazil) for providing HPC resources for the SDumont supercomputer, contributing to the research results reported in this paper.

Appendix A. Supplementary data

Supplementary material related to this article can be found online at https://doi.org/10.1016/j.est.2025.116099.

Data availability

No data was used for the research described in the article.

References

[1] A. Hirsch, The era of carbon allotropes, Nat. Mater. 9 (11) (2010) 868–871.
[2] S. Nasir, M.Z. Hussein, Z. Zainal, N.A. Yusof, Carbon-based nanomaterials/allotropes: A glimpse of their synthesis, properties and some applications, Materials 11 (2) (2018) 295.
[3] H. Lu, S.-D. Li, Two-dimensional carbon allotropes from graphene to graphyne, J. Mater. Chem. C 1 (23) (2013) 3677–3680.
[4] S.K. Tiwari, V. Kumar, A. Huczko, R. Oraon, A.D. Adhikari, G. Nayak, Magical allotropes of carbon: prospects and applications, Crit. Rev. Solid State Mater. Sci. 41 (4) (2016) 257–317.
[5] W.-c. Yi, W. Liu, J. Botana, J.-y. Liu, M.-s. Miao, Microporosity as a new property control factor in graphene-like 2D allotropes, J. Mater. Chem. A 6 (22) (2018) 10348–10353.
[6] X. Fan, J. Li, G. Chen, New carbon allotropes with metallic conducting properties: a first-principles prediction, RSC Adv. 7 (28) (2017) 17417–17426.
[7] L.F.C. Pereira, Investigating mechanical properties and thermal conductivity of 2D carbon-based materials by computational experiments, Comput. Mater. Sci. 196 (2021) 110493.
[8] S.-Y. Yue, G. Qin, X. Zhang, X. Sheng, G. Su, M. Hu, Thermal transport in novel carbon allotropes with sp 2 or sp 3 hybridization: An ab initio study, Phys. Rev. B 95 (8) (2017) 085207.
[9] J. Zhao, N. Wei, Z. Fan, J.-W. Jiang, T. Rabczuk, The mechanical properties of three types of carbon allotropes, Nanotechnology 24 (9) (2013) 095702.
[10] S. Singhal, M. Gupta, M.S. Alam, M.N. Javed, J.R. Ansari, Carbon allotropes-based nanodevices: graphene in biomedical applications, in: Nanotechnology, CRC Press, 2022, pp. 241–269.
[11] A. Rajkamal, R. Thapa, Carbon allotropes as anode material for lithium-ion batteries, Adv. Mater. Technol. 4 (10) (2019) 1900307.
[12] A. Lherbier, G. Vander Marcken, B. Van Troeye, A.R. Botello-Méndez, J.-J. Adjizian, G. Hautier, X. Gonze, G.-M. Rignanese, J.-C. Charlier, Lithiation properties of sp 2 carbon allotropes, Phys. Rev. Mater. 2 (8) (2018) 085408.
[13] G. Wang, M. Yu, X. Feng, Carbon materials for ion-intercalation involved rechargeable battery technologies, Chem. Soc. Rev. 50 (4) (2021) 2388–2443.
[14] H.G. Ali, K. Khan, M.B. Hanif, M.Z. Khan, I. Hussain, M.S. Javed, H.A. AL-bonsrulah, M. Mosiałek, M. Fichtner, M. Motola, Advancements in two-dimensional materials as anodes for lithium-ion batteries: Exploring composition-structure-property relationships emerging trends, and future perspective, J. Energy Storage 73 (2023) 108980.
[15] A.P. Cocco, G.J. Nelson, W.M. Harris, A. Nakajo, T.D. Myles, A.M. Kiss, J.J. Lombardo, W.K. Chiu, Three-dimensional microstructural imaging methods for energy materials, Phys. Chem. Chem. Phys. 15 (39) (2013) 16377–16407.
[16] V.G. Desyatkin, W.B. Martin, A.E. Aliev, N.E. Chapman, A.F. Fonseca, D.S. Galvão, E.R. Miller, K.H. Stone, Z. Wang, D. Zakhidov, et al., Scalable synthesis and characterization of multilayer γ-graphyne, new carbon crystals with a small direct band gap, J. Am. Chem. Soc. 144 (39) (2022) 17999–18008.
[17] X. Gao, H. Liu, D. Wang, J. Zhang, Graphdiyne: synthesis, properties, and applications, Chem. Soc. Rev. 48 (3) (2019) 908–936.
[18] Q. Song, B. Wang, K. Deng, X. Feng, M. Wagner, J.D. Gale, K. Müllen, L. Zhi, Graphenylene, a unique two-dimensional carbon network with nondelocalized cyclohexatriene units, J. Mater. Chem. C 1 (1) (2013) 38–41.
[19] Y.-X. Yu, Graphenylene: a promising anode material for lithium-ion batteries with high mobility and storage, J. Mater. Chem. A 1 (43) (2013) 13559–13566.
[20] M. Ruby Raj, G. Lee, M.V. Reddy, K. Zaghib, Recent advances in development of organic battery materials for monovalent and multivalent metal-ion rechargeable batteries, ACS Appl. Energy Mater. 7 (19) (2024) 8196–8255.
[21] M. Li, J. Lu, Z. Chen, K. Amine, 30 years of lithium-ion batteries, Adv. Mater. 30 (33) (2018) 1800561.
[22] M. Wakihara, Recent developments in lithium ion batteries, Mater. Sci. Eng.: R: Rep. 33 (4) (2001) 109–134.
[23] T. Kim, W. Song, D.-Y. Son, L.K. Ono, Y. Qi, Lithium-ion batteries: outlook on present, future, and hybridized technologies, J. Mater. Chem. A 7 (7) (2019) 2942–2964.
[24] B. Scrosati, J. Hassoun, Y.-K. Sun, Lithium-ion batteries. a look into the future, Energy & Environ. Sci. 4 (9) (2011) 3287–3295.
[25] G.E. Blomgren, The development and future of lithium ion batteries, J. Electrochem. Soc. 164 (1) (2016) A5019.
[26] A. Manthiram, An outlook on lithium ion battery technology, ACS Central Sci. 3 (10) (2017) 1063–1069.
[27] J. Gomez Quispe, B. Ipaves, D.S. Galvao, P.A.d.S. Autreto, TPDH-graphene as a new anodic material for lithium ion battery: DFT-based investigations, ACS Omega 9 (37) (2024) 39195–39201.
[28] S. Wang, B. Yang, H. Chen, E. Ruckenstein, Popgraphene: a new 2D planar carbon allotrope composed of 5–8–5 carbon rings for high-performance lithium-ion battery anodes from bottom-up programming, J. Mater. Chem. A 6 (16) (2018) 6815–6821.
[29] E. Santos, K. Lima, L. Ribeiro Junior, Proposing TODD-graphene as a novel porous 2D carbon allotrope designed for superior lithium-ion battery efficiency, Sci. Rep. 14 (1) (2024) 6202.
[30] D. Li, Two-dimensional c 5678: A promising carbon-based high-performance lithium-ion battery anode, Mater. Adv. 2 (1) (2021) 398–402.
[31] H. Liu, Y. Wei, D. Wu, S. Wang, A novel 2D carbon allotrope for high-performance metal-ion battery anode material, Mater. Sci. Semicond. Process. 173 (2024) 108146.
[32] X. Li, Q. Wang, P. Jena, ψ-Graphene: a new metallic allotrope of planar carbon with potential applications as anode materials for lithium-ion batteries, J. Phys. Chem. Lett. 8 (14) (2017) 3234–3241.
[33] Y. Cai, Y. Wei, C. Lv, L. Zhang, Y. Chen, LC 567: a new 2D semimetallic carbon allotrope as a promising anode material for lithium-ion batteries, Phys. Chem. Chem. Phys. 25 (28) (2023) 19239–19244.
[34] K. Lu, T. Wang, X. Li, L. Dai, J. Yin, Y. Ding, A new 2D carbon allotrope C568 as a high-capacity electrode material for lithium-ion batteries, Fullerenes, Nanotub. Carbon Nanostruct. 30 (3) (2022) 385–391.
[35] X.H. Cai, Q. Yang, S. Zheng, M. Wang, Net-C18: A predicted two-dimensional planar carbon allotrope and potential for an anode in lithium-ion battery, Energy & Environ. Mater. 4 (3) (2021) 458–464.
[36] Z. Cheng, X. Zhang, H. Zhang, J. Gao, H. Liu, X. Yu, X. Dai, G. Liu, G. Chen, Two-dimensional metallic carbon allotrope with multiple rings for ion batteries, Phys. Chem. Chem. Phys. 23 (34) (2021) 18770–18776.
[37] M. You, G. Guo, Y. Liao, S. Luo, C. He, C. Tang, J. Zhong, 2D novel C5N2 allotropes: High-performance anode materials for alkali metal ion battery, J. Energy Storage 84 (2024) 111004.
[38] J. Liu, T. Zhao, S. Zhang, Q. Wang, A new metallic carbon allotrope with high stability and potential for lithium ion battery anode material, Nano Energy 38 (2017) 263–270.
[39] W. Wang, J. Meng, Y. Hu, J. Wang, Q. Li, J. Yang, Thgraphene: a novel two-dimensional carbon allotrope as a potential multifunctional material for electrochemical water splitting and potassium-ion batteries, J. Mater. Chem. A 10 (18) (2022) 9848–9857.
[40] E. Santos, K. Lima, F. Mendonça, D.d. Silva, W. Giozza, L.R. Junior, PHOTH-graphene: A new 2D carbon allotrope with low barriers for Li-ion mobility, Sci. Rep. 14 (1) (2024) 9526.
[41] Z. Liu, Y. Tian, P. Wang, G. Zhang, Applications of graphene-based composites in the anode of lithium-ion batteries, Front. Nanotechnol. 4 (2022) 952200.
[42] A.R. Puigdollers, G. Alonso, P. Gamallo, First-principles study of structural, elastic and electronic properties of α-, β-and γ-graphyne, Carbon 96 (2016) 879–887.
[43] L. Hou, X. Cui, B. Guan, S. Wang, R. Li, Y. Liu, D. Zhu, J. Zheng, Synthesis of a monolayer fullerene network, Nature 606 (7914) (2022) 507–510.
[44] Z. Wang, X.-F. Zhou, X. Zhang, Q. Zhu, H. Dong, M. Zhao, A.R. Oganov, Phagraphene: a low-energy graphene allotrope composed of 5–6–7 carbon rings with distorted dirac cones, Nano Lett. 15 (9) (2015) 6182–6186.
[45] Z. Zhuo, X. Wu, J. Yang, Me-graphene: a graphene allotrope with near zero Poisson's ratio, sizeable band gap, and high carrier mobility, Nanoscale 12 (37) (2020) 19359–19366.
[46] D.H. Lo, M. Whitehead, Pyracyclene: neutral, dication, and dianion, Chem. Commun. (London) (14) (1968) 771–772.
[47] B.M. Trost, G.M. Bright, Pyracylene. Pentalenoid system, J. Am. Chem. Soc. 89 (16) (1967) 4244–4245.
[48] S.J. Clark, M.D. Segall, C.J. Pickard, P.J. Hasnip, M.I. Probert, K. Refson, M.C. Payne, First principles methods using CASTEP, Z. Für Kristallographie- Cryst. Mater. 220 (5–6) (2005) 567–570.
[49] J.P. Perdew, K. Burke, M. Ernzerhof, Generalized gradient approximation made simple, Phys. Rev. Lett. 77 (1996) 3865.
[50] S. Grimme, Semiempirical GGA-type density functional constructed with a long-range dispersion correction, J. Comput. Chem. 27 (15) (2006) 1787–1799.
[51] S. Nosé, A unified formulation of the constant temperature molecular dynamics methods, J. Chem. Phys. 81 (1984) 511–519.
[52] K.L. Lima, L.R. Junior, A DFT study on the mechanical, electronic, thermodynamic, and optical properties of GaN and AlN counterparts of biphenylene network, Mater. Today Commun. 37 (2023) 107183.

[53] S. Makri, C. Ortner, J.R. Kermode, A preconditioning scheme for minimum energy path finding methods, J. Chem. Phys. 150 (9) (2019).
[54] J. Barzilai, J.M. Borwein, Two-point step size gradient methods, IMA J. Numer. Anal. 8 (1) (1988) 141–148.
[55] E. Bitzek, P. Koskinen, F. Gähler, M. Moseler, P. Gumbsch, Structural relaxation made simple, Phys. Rev. Lett. 97 (17) (2006) 170201.
[56] N. Metropolis, A.W. Rosenbluth, M.N. Rosenbluth, A.H. Teller, E. Teller, Equation of state calculations by fast computing machines, J. Chem. Phys. 21 (6) (1953) 1087–1092.
[57] S. Kirkpatrick, C.D. Gelatt Jr., M.P. Vecchi, Optimization by simulated annealing, Science 220 (4598) (1983) 671–680.
[58] V. Černỳ, Thermodynamical approach to the traveling salesman problem: An efficient simulation algorithm, J. Optim. Theory Appl. 45 (1985) 41–51.
[59] S. Plimpton, Fast parallel algorithms for short-range molecular dynamics, J. Comput. Phys. 117 (1995) 1–19.
[60] B. Mortazavi, M. Silani, E.V. Podryabinkin, T. Rabczuk, X. Zhuang, A.V. Shapeev, First-principles multiscale modeling of mechanical properties in graphene/borophene heterostructures empowered by machine-learning interatomic potentials, Adv. Mater. 33 (35) (2021) 2102807.
[61] I.S. Novikov, K. Gubaev, E.V. Podryabinkin, A.V. Shapeev, The MLIP package: moment tensor potentials with MPI and active learning, Mach. Learn.: Sci. Technol. 2 (2) (2020) 025002.
[62] E.V. Podryabinkin, A.V. Shapeev, Active learning of linearly parametrized interatomic potentials, Comput. Mater. Sci. 140 (2017) 171–180.
[63] G. Kresse, J. Hafner, Ab initio molecular dynamics for liquid metals, Phys. Rev. B 47 (1) (1993) 558.
[64] G. Kresse, J. Furthmüller, Efficiency of ab-initio total energy calculations for metals and semiconductors using a plane-wave basis set, Comput. Mater. Sci. 6 (1) (1996) 15–50.
[65] G. Kresse, J. Hafner, Norm-conserving and ultrasoft pseudopotentials for first-row and transition elements, J. Phys.: Condens. Matter. 6 (40) (1994) 8245.
[66] B. Mortazavi, Machine learning interatomic potentials: Keys to first-principles multiscale modeling, in: Machine Learning in Modeling and Simulation: Methods and Applications, Springer, 2023, pp. 427–451.
[67] B. Mortazavi, T. Rabczuk, X. Zhuang, Exploring the structural stability, thermal and mechanical properties of nanoporous carbon nitride nanosheets using a transferrable machine learning interatomic potential, Mach. Learn. Comput. Sci. Eng. 1 (1) (2025) 5.
[68] B. Mortazavi, X. Zhuang, T. Rabczuk, A.V. Shapeev, Atomistic modeling of the mechanical properties: the rise of machine learning interatomic potentials, Mater. Horizons 10 (6) (2023) 1956–1968.
[69] B. Mortazavi, E.V. Podryabinkin, I.S. Novikov, S. Roche, T. Rabczuk, X. Zhuang, A.V. Shapeev, Efficient machine-learning based interatomic potentialsfor exploring thermal conductivity in two-dimensional materials, J. Phys.: Mater. 3 (2) (2020) 02LT02.
[70] B. Mortazavi, Electronic, thermal and mechanical properties of carbon and boron nitride holey graphyne monolayers, Materials 16 (20) (2023) 6642.
[71] B. Mortazavi, Goldene: An anisotropic metallic monolayer with remarkable stability and rigidity and low lattice thermal conductivity, Materials 17 (11) (2024) 2653.
[72] K.A. Lima, R.A. Alves, D.A. da Silva, F.L. Mendonça, M.L. Pereira, L.A. Ribeiro, TH-graphyne: a new porous bidimensional carbon allotrope, Phys. Chem. Chem. Phys. (2024).
[73] B. Mortazavi, I.S. Novikov, A.V. Shapeev, A machine-learning-based investigation on the mechanical/failure response and thermal conductivity of semiconducting BC2N monolayers, Carbon 188 (2022) 431–441.
[74] B. Mortazavi, A.V. Shapeev, Anisotropic mechanical response, high negative thermal expansion, and outstanding dynamical stability of biphenylene monolayer revealed by machine-learning interatomic potentials, FlatChem 32 (2022) 100347.
[75] Y. Luo, C. Ren, Y. Xu, J. Yu, S. Wang, M. Sun, A first principles investigation on the structural, mechanical, electronic, and catalytic properties of biphenylene, Sci. Rep. 11 (1) (2021) 19008.
[76] S.T. Skowron, I.V. Lebedeva, A.M. Popov, E. Bichoutskaia, Energetics of atomic scale structure changes in graphene, Chem. Soc. Rev. 44 (10) (2015) 3143–3176.
[77] R.M. Tromer, M.L. Pereira Junior, K.A. L. Lima, A.F. Fonseca, L.R. da Silva, D.S. Galvao, L.A. Ribeiro Junior, Mechanical, electronic, and optical properties of 8-16-4 graphyne: A 2d carbon allotrope with dirac cones, J. Phys. Chem. C 127 (25) (2023) 12226–12234.
[78] M.P. Junior, W.F. da Cunha, W.F. Giozza, R.T. de Sousa Junior, L.R. Junior, Irida-graphene: A new 2d carbon allotrope, FlatChem 37 (2023) 100469.
[79] K. Lima, F.F. Monteiro, E. Santos, R. Alves, W.F. Giozza, L.R. Junior, Dodecanophene: A novel 2D carbon allotrope with untunable metallic behavior under stress, Mater. Today Commun. (2024) 109455.
[80] M. Zhao, W. Dong, A. Wang, Two-dimensional carbon topological insulators superior to graphene, Sci. Rep. 3 (1) (2013) 3532.
[81] B. Mortazavi, I.S. Novikov, E.V. Podryabinkin, S. Roche, T. Rabczuk, A.V. Shapeev, X. Zhuang, Exploring phononic properties of two-dimensional materials using machine learning interatomic potentials, Appl. Mater. Today 20 (2020) 100685.
[82] F. Scarpa, S. Adhikari, A.S. Phani, Effective elastic mechanical properties of single layer graphene sheets, Nanotechnology 20 (6) (2009) 065709.
[83] J.-U. Lee, D. Yoon, H. Cheong, Estimation of Young's modulus of graphene by Raman spectroscopy, Nano Lett. 12 (9) (2012) 4444–4448.
[84] H. Lian, A.N. Christiansen, D. Tortorelli, O. Sigmund, N. Aage, Combined shape and topology optimization for minimization of maximal von Mises stress, Struct. Multidiscip. Optim. 55 (2017) 1541–1557, http://dx.doi.org/10.1007/s00158-017-1656-x.
[85] Y.-F. Zhang, J. Guo, Li-decorated 2d irida-graphene as a potential hydrogen storage material: A dispersion-corrected density functional theory calculations, Int. J. Hydrog. Energy 50 (2024) 1004–1014.
[86] D. Kim, S. Lee, Y. Hwang, K.-H. Yun, Y.-C. Chung, Hydrogen storage in Li dispersed graphene with Stone–Wales defects: a first-principles study, Int. J. Hydrog. Energy 39 (25) (2014) 13189–13194.
[87] J. Dewangan, V. Mahamiya, A. Shukla, B. Chakraborty, Lithium decorated ψ-graphene as a potential hydrogen storage material: density functional theory investigations, Int. J. Hydrog. Energy 48 (96) (2023) 37908–37920.
[88] L. Bi, Z. Miao, Y. Ge, Z. Liu, Y. Xu, J. Yin, X. Huang, Y. Wang, Z. Yang, Density functional theory study on hydrogen storage capacity of metal-embedded penta-octa-graphene, Int. J. Hydrog. Energy 47 (76) (2022) 32552–32564.
[89] P. Álvarez-Zapatero, A. Herrero, A. Lebon, L. Gallego, A. Vega, Ab initio study of lithium decoration of popgraphene and hydrogen storage capacity of the hybrid nanostructure, Int. J. Hydrog. Energy 46 (29) (2021) 15724–15737.
[90] G. Wu, S. Gao, C. Zhang, X. Zhang, J. Hao, B. Jia, X. Guan, Potential hydrogen storage materials from Li decorated N-doped Me-graphene, Int. J. Energy Res. 46 (15) (2022) 24554–24564.
[91] X. Wang, Z. Feng, J. Rong, Y. Zhang, Y. Zhong, J. Feng, X. Yu, Z. Zhan, Planar net-π: A new high-performance metallic carbon anode material for lithium-ion batteries, Carbon 142 (2019) 438–444.
[92] Y. Shaidu, E. Kucukbenli, S. De Gironcoli, Lithium adsorption on graphene at finite temperature, J. Phys. Chem. C 122 (36) (2018) 20800–20808.
[93] J. He, Z. Jiao, MoS2/C3N heterostructure: a promising anode material for Lithium-ion batteries, Appl. Surf. Sci. 580 (2022) 152371.
[94] G. Kucinskis, G. Bajars, J. Kleperis, Graphene in lithium ion battery cathode materials: A review, J. Power Sources 240 (2013) 66–79.
[95] G. Wang, X. Shen, J. Yao, J. Park, Graphene nanosheets for enhanced lithium storage in lithium ion batteries, Carbon 47 (8) (2009) 2049–2053.
[96] F. Liu, S. Song, D. Xue, H. Zhang, Folded structured graphene paper for high performance electrode materials, Adv. Mater. (Deerfield Beach, Fla.) 24 (8) (2012) 1089–1094.
[97] K. Persson, Y. Hinuma, Y.S. Meng, A. Van der Ven, G. Ceder, Thermodynamic and kinetic properties of the Li-graphite system from first-principles calculations, Phys. Rev. B— Condens. Matter Mater. Phys. 82 (12) (2010) 125416.
[98] S. Gao, E. Abduryim, C. Chen, C. Dong, X. Guan, S. Guo, Y. Kuai, G. Wu, W. Chen, P. Lu, Twin-graphene: a promising anode material for lithium-ion batteries with ultrahigh specific capacity, J. Phys. Chem. C 127 (29) (2023) 14065–14074.
[99] T.-C. Qiu, Z.-G. Shao, C.-L. Wang, L. Yang, QPHT graphene as a high-performance lithium ion battery anode materials with low diffusion barrier and high capacity, Phys. Lett. A 456 (2022) 128549.
[100] S. Bagheri, A. Shameli, M. Darvishi, G. Fakhrpour, Molecular investigation of water adsorption on graphene and graphyne surfaces, Phys. E: Low- Dimens. Syst. Nanostructures 90 (2017) 123–130.
[101] H. de Araujo Chagas, E.E. Fileti, G. Colherinhas, A molecular dynamics study of graphyne-based electrode and biocompatible ionic liquid for supercapacitor applications, J. Mol. Liq. 360 (2022) 119494.
[102] C.-Y. Lee, K.-W. Sung, H.-J. Ahn, Electrochemical properties of heteroatom doped graphyne sheet for energy storage devices, J. Energy Storage 109 (2025) 115064.